Check for updates

Received: 23 February 2022 | Revised: 13 August 2022 | Accepted: 20 August 2022

DOI: 10.1002/er.8690

SPECIAL ISSUE RESEARCH ARTICLE

INTERNATIONAL JOURNAL OF ENERGY RESEARCH WILEY

Optimization of the ratio of aniline, ammonium persulfate, *para*-toluenesulfonic acid for the synthesis of conducting polyaniline and its use in energy storage devices

Tapas Das | Vikas Kumar Pandey | Sanjeev Verma | Saurabh Kumar Pandey | Bhawna Verma

Department of Chemical Engineering & Technology, IIT BHU, Varanasi, India

Correspondence
Bhawna Verma, Department of Chemical Engineering & Technology, IIT BHU, Varanasi 221005, India.
Email: bverma.che@itbhu.ac.in

Funding information
Ministry of Human Resource Development

Summary

We have successfully synthesized *para*-toluenesulfonic acid (PTSA)-based conducting polyaniline (PA) by using ammonium persulfate (APS) as oxidant for supercapacitor electrode applications. The primary aim is to find out the optimized ratio of APS:aniline and aniline:PTSA based on the electrochemical performances of the fabricated electrodes. PA having APS:aniline ratio of 1.25:1 and aniline:PTSA ratio of 2:1 exhibited the highest value of specific capacitance, specific energy, specific power, and coulombic efficiency of 82.22 F/g, 11.42 Wh/kg, 124.99 W/kg, and 95.95%, respectively. It offers very low charge transfer resistance of 3.1 Ω during the electrochemical processes. The cycle life of the corresponding system is the largest among all, which is 88.97% retention after 2000 cycles. The robust electrochemical behavior may be due to the uniform rod-shaped morphology of the corresponding system, which may be providing seamless movement of the electrolyte ions to the electrochemical active sites along with proper electrical connection.

KEYWORDS

coulombic efficiency, *para*-toluenesulfonic acid, polyaniline, specific power, supercapacitor

1 | INTRODUCTION

The increasing demands of energy storage devices have been rising due to the requirement of energy in every sector. Supercapacitors having high energy and power density, high specific capacitance, high reversibility, outstanding cycle stability are setting benchmark in the field of energy storage devices. The functioning of supercapacitors could be electrical double layer capacitance (EDLC) or pseudocapacitive in nature based on the materials used in the electrodes. Carbon-based materials store charge by the process of surface adsorption by creating double layers of opposite charges. They exhibit very less specific capacitance and energy density. Metal oxides and conducting polymers undergo redox transitions and attribute pseudocapacitive nature. So, they have high specific capacitance and energy density, but substandard cycle life due to expansion-contraction during charge-discharge (CD) process. Metal oxides have another drawback of having inferior conductivity. Polyaniline (PANI) is being evolved as an excellent candidate for supercapacitor electrodes due to its high capacitance, electrical conductivity, environmental stability, storage ability, and low cost.[1-3] The electrical conductivity of PANI comes from the π-conjugated system and various resonance structure. PANI has three oxidation states: pernigraniline (fully oxidized), emeraldine base (EB) (half oxidized), and leucoemeraldine (fully reduced). Out of all these forms, EB has

 © 2022 John Wiley & Sons Ltd.

the maximum stability, which has equal number of –NH– group (reduced amine) and –N═ group (oxidized imine). In general, it is very less conducting due to a very large band gap, but can be transformed to a conducting form (emeraldine salt [ES]) by doping with desired acid. During the protonation of EB, the polymer backbone gets charged positively and the surrounding of polymeric chains are occupied by negative counterions, resulting PANI ES. This will bring a change in the conjugation length of PANI and will enhance the conductivity along with the electrochemical activities significantly.[4,5] The electrochemical performances of PANI can be enhanced by doping with various protic molecules like DBSA, CSA, *para*-toluenesulfonic acid (PTSA), and so forth along with the use of proper oxidizing agents like $(NH_4)_2S_2O_8$, $K_2Cr_2O_7$, $K_3[Fe(CN)_6]$, and so forth. These dopant acids contain sulfonate group that is negatively charged and this group move toward positively charged PANI backbone by coulombic attraction. The role of oxidizing agent is to propagate polymerization reaction by creating free radicals.[6,7]

PANI can be synthesized by chemical oxidative polymerization, emulsion polymerization, interfacial polymerization, electrochemical polymerization, and so forth of aniline. Out of all the techniques, chemical oxidative polymerization is extensively used due to the ease of synthesis, yield, cost effectiveness, and better purity of the products.[8,9] Performance of the supercapacitor electrodes rely on various parameters like oxidant used, dopant used, monomer to oxidant molar ratio, monomer to dopant molar ratio, pH, polymerization temperature and time, and so forth. So, it is very essential to find out the optimized values of these parameters to get an efficient supercapacitor electrode.[10,11] A lot of researches have been done on the effect of pH, polymerization time and temperature on the electrochemical performances of PANI. Acidic pH is favourable for PANI synthesis. Low synthesis temperature (−40°C to 5°C) gives better yield and electrochemical properties of the synthesized PANI. A moderate range of polymerization time of 10 to 24 h gives better yield during the synthesis of PANI.[12-14] In the current research, we have used PTSA to dope sulfur in PANI and prepare rod-shaped PANI. We have used ammonium persulfate (APS) as an oxidizing agent in the current work. We have also optimized the molar ratios of oxidant to monomer (aniline) and monomer to dopant on the basis of electrochemical performances. To the best of our knowledge, there is no report on the optimization of aniline:PTSA and APS:aniline molar ratio in such a wide range. APS is an oxidizing agent which plays a big role in the polymerization of aniline. So, the ratio is important as an appropriate proportion can inhibit the formation of oligomers.

2 | EXPERIMENTAL SECTION

2.1 | Materials

Aniline, nafion, 2-propanol, carbon paper, and conductive silver paste were purchased from Alfa aesar. PTSA and APS were taken from Sisco Research Laboratories Private Limited. All the materials were analytical grade (ACS grade) and no purification was required before use.

2.2 | Synthesis of PTSA-based PANI

All the PANI samples were synthesized by chemical oxidative polymerization reaction by taking APS as an oxidant (initiator) and PTSA as a dopant. In Table 1, the experimental molar ratio of aniline:PTSA and APS:aniline have been provided. Desired amount of PTSA and APS were completely dissolved in double distilled water and kept at 0°C to 4°C along with aniline of required quantity. Then, ice bath was used to maintain the temperature at 0°C to 4°C throughout the process. Initially, aniline was released dropwise into the previously prepared PTSA solution followed by stirring for half an hour. To initiate the polymerization reaction, APS solution was added tardily to the aniline-PTSA solution. This polymerization process is exothermic in nature; so, a very slow addition of APS was done not to allow any abrupt rise in temperature. Initially the solution was brownish in color and eventually changed to dark green precipitates after complete addition of APS solution. The resulting mixture (precipitate) was stirred for 1 h, kept in a refrigerator for 12 h followed by vacuum filtration and vacuum drying at 60°C for 5 h.[15] Figure S1a,b represent the experimental set-up for synthesis and different redox states of PANI.

2.3 | Electrode and supercapacitor fabrication

Copper wire was taken to be used as a current collector with one site flattened and keeping the other side as it was. The flattened side was connected to a carbon paper substrate by using conductive silver glue. A homogeneous slurry of 5 mg PANI, 12 μL nafion, 0.2 mL of 2-propanol was prepared and drop casted on the substrate uniformly. Then the electrode was left in the normal atmospheric conditions till it was completely dried. Copper wire was connected to carbon paper substrate (area 1 cm^2) with the help of conductive silver glue. The active material was drop casted on the carbon paper substrate. The mass loading was kept at 2 mg/cm^2. To check the reliability and stability of the electrodes, symmetric

1099114x, 2022, 14, Downloaded from https://onlinelibrary.wiley.com/doi/10.1002/er.8690 by Indian Institute Of Technology, Wiley Online Library on [18/04/2023]. See the Terms and Conditions (https://onlinelibrary.wiley.com/terms-and-conditions) on Wiley Online Library for rules of use; OA articles are governed by the applicable Creative Commons License

TABLE 1 Experimental data and electrochemical outputs of all the systems

Samples	Aniline: PTSA	APS: Aniline	(CV 3E) C_{SP} (F/g)	(CV 2E) C_{SP} (F/g)	(CD 2E) C_{SP} (F/g)	% CE	E_S (Wh/kg)	E_P (W/kg)	R_{CT} (Ω)	% Retention
PA1	1:2	1:1	141.22	41.85	36.64	84.13	5.08	124.75	23	75.13
PA2	1:0	1:1	135.78	38.37	33.69	84.13	4.67	124.75	20	74.55
PA3	2:1	1:1	159.74	46.26	41.31	85.12	5.73	124.81	11.1	76.16
PA4	4:1	1:1	152.54	42.3	38.52	84.48	5.35	124.97	13.2	75.67
PA5	1:2	1.05:1	112.2	29.89	26.37	81.08	3.66	124.86	69	68.16
PA6	1:4	1.05:1	102.54	27.06	20.78	78.93	2.88	124.7	79.2	62.97
PA7	2:1	1.05:1	125.62	37.66	31.58	81.97	4.38	124.81	42	73.09
PA8	4:1	1.05:1	115.24	33.72	29.11	81.97	4.04	124.9	56	71.3
PA9	1:2	1.1:1	172.62	53.45	45.02	85.94	6.25	124.92	7.5	78.61
PA10	1:4	1.1:1	163.31	47.34	43.34	85.71	6.02	124.99	21	77.23
PA11	2:1	1.1:1	187.79	60.83	52.58	87.67	7.3	124.94	8.3	79.65
PA12	4:1	1.1:1	179.08	56.46	49.69	87.01	6.9	124.96	6.1	79.17
PA13	1:2	1.15:1	207.33	75.19	57.16	88.33	7.93	124.85	7.1	80.81
PA14	1:4	1.15:1	197.4	71.3	55.31	88.33	7.68	124.94	8.7	80.26
PA15	2:1	1.15:1	220.79	81.07	60.79	89.67	8.44	124.95	13.8	81.52
PA16	4:1	1.15:1	215.24	78.66	57.64	89	8	124.9	10.6	81.13
PA17	1:2	1.2:1	239.58	88.64	66.73	91.72	9.26	124.88	6.7	83.58
PA18	1:4	1.2:1	229.66	87	63.78	90.35	8.85	124.87	14.5	82.02
PA19	2:1	1.2:1	256.83	97.79	71.26	93.11	9.89	124.89	7.7	85.93
PA20	4:1	1.2:1	251.42	93.18	69.49	92.41	9.65	124.97	8.7	84.76
PA21	1:2	1.25:1	285.44	106.86	77.94	95.23	10.82	124.93	3.9	87.63
PA22	1:4	1.25:1	274.9	104.54	75.86	94.52	10.53	124.92	4.2	87.06
PA23	2:1	1.25:1	301.49	119.84	82.22	95.95	11.42	124.99	3.1	88.97
PA24	4:1	1.25:1	289.87	111.7	80.52	95.95	11.18	124.95	3.6	88.13
PA25	1:2	1.3:1	246.92	91.26	67.79	92.41	9.41	124.91	5.7	84.19
PA26	1:4	1.3:1	236.47	87.61	62.78	91.03	8.71	124.86	8.8	82.46
PA27	2:1	1.3:1	261.34	99.79	72.78	93.81	10.1	124.88	4.6	86.21
PA28	4:1	1.3:1	255.66	96.95	70.85	93.11	9.84	124.99	6.5	85.43

supercapacitors were fabricated by taking two equal electrodes (as anode and cathode), Whatman filter paper as semipermeable membrane, and potassium hydroxide (KOH) as electrolyte. Schematic of the electrode and supercapacitor have been provided in Figure S2a,b.

2.4 | Electrochemical and material characterizations

The main purpose of this work is to find out the best molar ratio of the constituents (APS:aniline and aniline: PTSA) on the basis of their electrochemical attributes. So, we performed cyclic voltammetry (CV), CD, electrochemical impedance spectroscopy (EIS) of all the samples. Then, we did the material characterizations of the best three and the worst two samples to correlate the electrochemical behavior with the microstructure.

The electrochemical testing was executed for the electrodes (three electrode configuration) and symmetric supercapacitors (two-electrode configuration) in 1 M KOH electrolyte with the help of VersaSTAT3. In the cell system, we took active material based electrode/supercapacitor as the working electrode, platinum electrode was taken as counter electrode which helps in completing the circuit and causes to flow the charges, Ag/AgCl electrode was taken as reference electrode which provides controlled and stable potential to the working electrode. CV and CD was done at 5 mV/s and 1 mA, respectively. Ten millivolts of AC amplitude was

1099114x, 2022, 14, Downloaded from https://onlinelibrary.wiley.com/doi/10.1002/er.8690 by Indian Institute Of Technology, Wiley Online Library on [18/04/2023]. See the Terms and Conditions (https://onlinelibrary.wiley.com/terms-and-conditions) on Wiley Online Library for rules of use; OA articles are governed by the applicable Creative Commons License

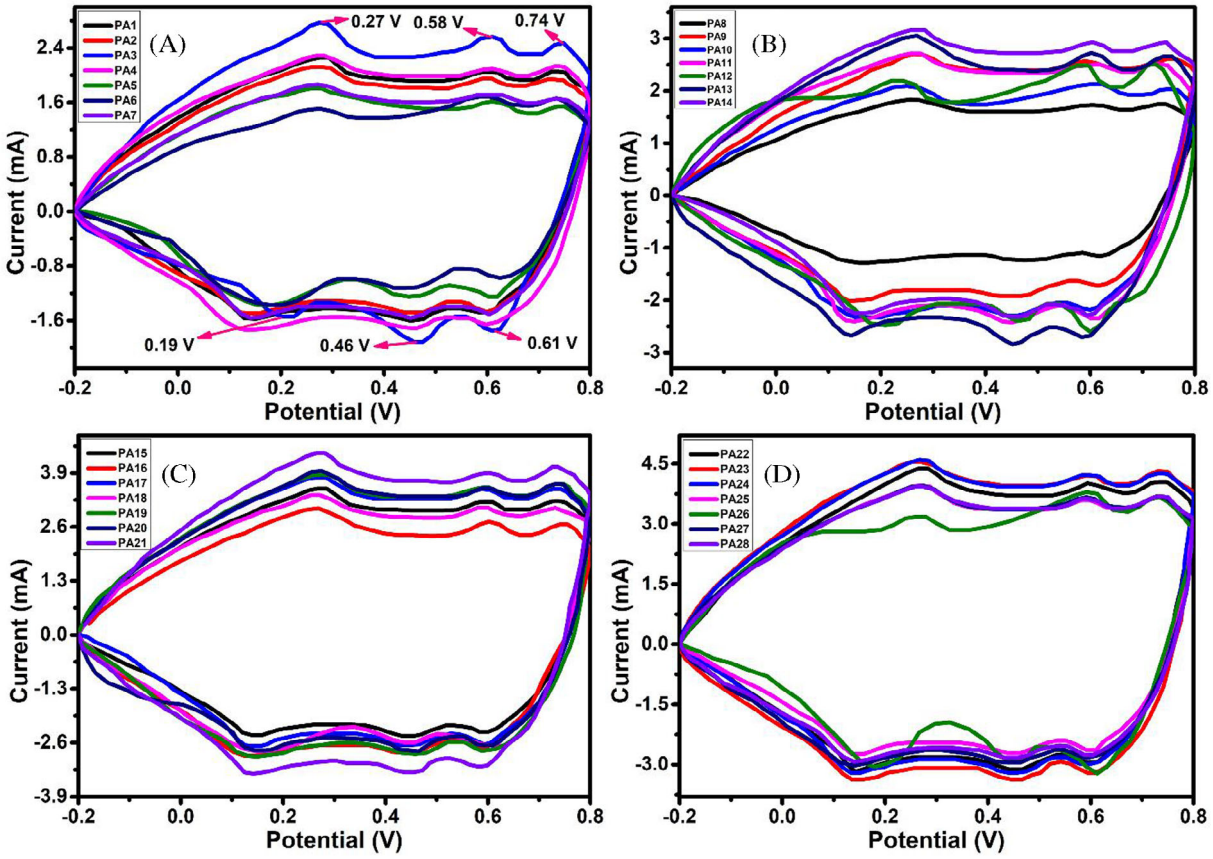

FIGURE 1 CV in 3E (three electrode) configuration

given over a frequency of 0.1 Hz to 100 kHz to execute EIS. The electrochemical performances at various concentrations have been provided in the Figure S12. In comparison to 0.5 and 2 M, 1 M concentration exhibited better CD behavior; so, we have taken 1 M KOH for further studies.

Crystalline natures of the synthesized materials were examined by Rigaku MiniFlex 600 desktop X-ray diffraction (XRD) system at 5°/min between $2\theta = 10°$ to 70° keeping $\lambda = 0.154$ nm. Nicolet iS5-Thermo Electron Scientific Instruments LLC was used to run Fourier transform infrared (FTIR) spectroscopy and recognize the functional groups existing in the material. Nova NanoSEM 450 (FEI Company of USA [S.E.A] Pte, Ltd) was used to perform microstructural analysis of PA23 by field-emission scanning electron microscopy (FESEM) technique. Elemental percentages of the constituents were estimated by EDS analysis performed by "Team Pegasus Integrated EDS-EBSD with octane plus and Hikari Pro equipped with the SEM machine". The micrograph of PA23 was captured by high-resolution (HR) transmission electron microscope (TEM) (Tecnai G2 20 TWIN; FEI Company of USA [S.E.A] Pte, Ltd) to obtain morphology of the synthesized composite. Phase identification of the components in the composite was accomplished by the selected area diffraction (SAED) pattern. Scanning probe microscopy or atomic force microscopy (AFM) was performed by NTEGRA prima to observe the surface roughness of the samples. Disc shaped pellets having 1-cm diameter was prepared and the measurements were executed at ambient pressure. The surface was scanned at a wide scanning area of 60 μm × 60 μm and the obtained data were analyzed by Nova Px software. The rheological study was carried out by MCR 72 (Anton Paar) at room temperature. The frequency sweeps were done at the shear rate range of 0 to 100 rad/s.

3 | RESULTS AND DISCUSSION

3.1 | Electrochemical characterizations

CV of all the electrodes and supercapacitors were done at a potential scan rate of 5 mV/s and the stability potential window was found to be 1 V (−0.2 to 0.8 V). Figure 1A-D demonstrate the CV plots of the working electrodes in three electrode systems. Similarly,

10991145x, 2022, 14, Downloaded from https://onlinelibrary.wiley.com/doi/10.1002/er.8690 by Indian Institute Of Technology, Wiley Online Library on [18/04/2023]. See the Terms and Conditions (https://onlinelibrary.wiley.com/terms-and-conditions) on Wiley Online Library for rules of use; OA articles are governed by the applicable Creative Commons License

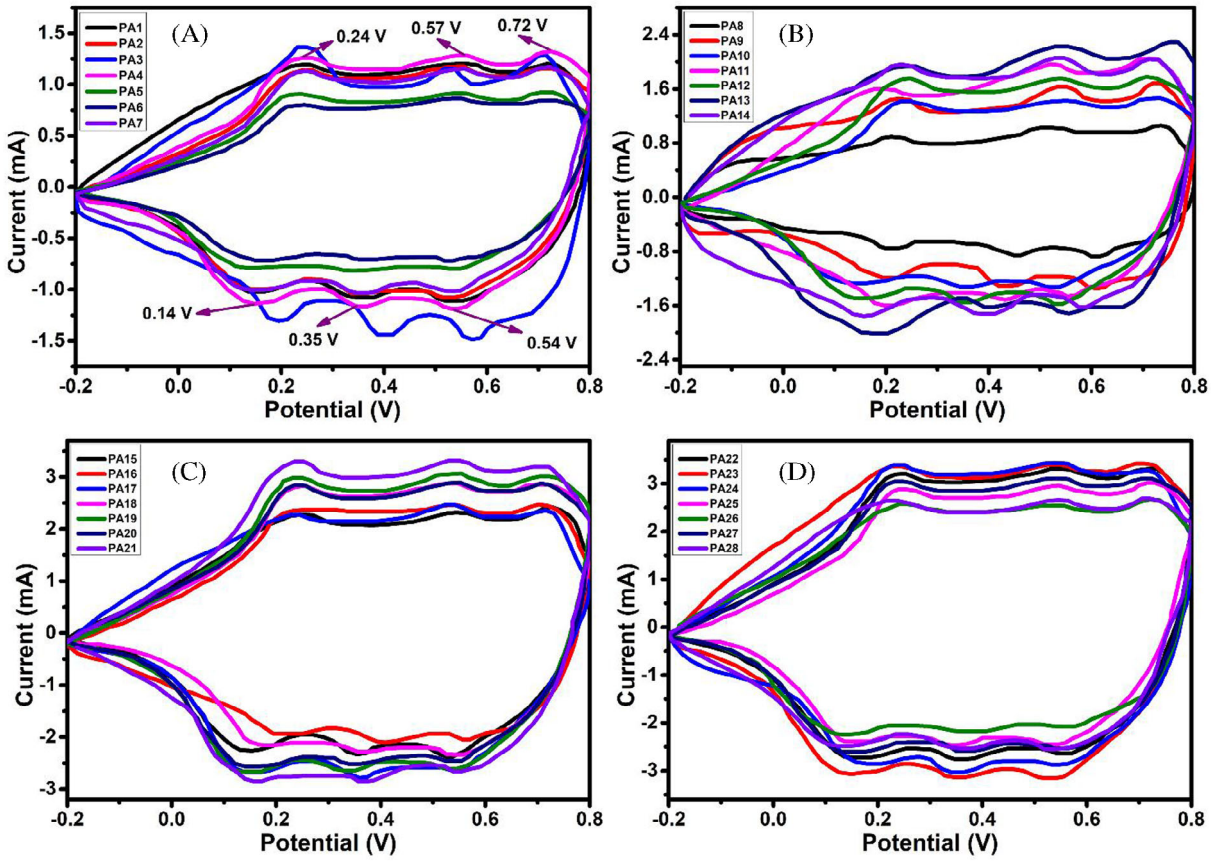

FIGURE 2 CV in 2E (two-electrode) configuration

Figure 2A-D represent the CV graphs of the fabricated supercapacitors. We applied a potential difference of 1 V and current was generated according to the conductivity of the active material. It can be seen that maximum current was generated for PA23 and the least current was generated for PA6. Table 1 contains various electrochemical properties of all the systems. In case of PA6 the ratio of APS:aniline (1.05:1) is low in compared to PA23 (1.25:1); so, there could be a possibility of the generation of more oligomers in PA6, which in turn restrict the flow of charges into the active sites due to discontinuous electrical network. In the synthesis process PTSA is used as a doping agent and its excessive loading could block the pores. In PA23 sample the aniline to PTSA ratio was kept at 2:1, which must be favoring the creation of proper texture of the sample. It is evident from the FESEM images that PA23 has a more uniform morphology than other samples, this could be the reason behind its excellent electrochemical behavior. In all the systems we can observe three redox peaks for PANI at approximately 0.27 V/0.19 V, 0.58 V/0.48 V, and 0.74 V/0.61 V.[16] The oxidation peak at 0.27 V is due to the conversion of leucoemeraldine salt to ES. At 0.58 V, degraded by products like benzoquinone/hydroquinone are formed. At 0.74 V potential, ES gets converted to pernigraniline (Figure S1b).

Equations (1) and (2) are used to calculate the specific capacitance from the CV data.

$$C_{SC,3E} = \frac{\int I \times dV}{M \times \nu \times \Delta V}, \quad (1)$$

$$C_{SC,2E} = \frac{\int I \times dV}{MT \times \nu \times \Delta V}, \quad (2)$$

$C_{SC,3E}$ and $C_{SC,2E}$ are the specific capacitances of three- and two-electrode systems (in F/g), respectively. $\int I \times dV$ is the area under cathodic scan, M refers to the mass of individual electrode (mg), MT is the sum of both electrodes, ν stands for the scan rate (in mV/s), and ΔV is the stable potential range (V). The calculated specific capacitance is the highest for PA23 in three- and two-electrode systems, that is, 301.49 and 119.84 F/g. So, on the basis of CV PA23 has the best ratio of the constituents.

CD of the supercapacitors were carried out at 1 mA (Figure 3A,B). All the systems have almost symmetric

1099114x, 2022, 14, Downloaded from https://onlinelibrary.wiley.com/doi/10.1002/er.8690 by Indian Institute Of Technology, Wiley Online Library on [18/04/2023]. See the Terms and Conditions (https://onlinelibrary.wiley.com/terms-and-conditions) on Wiley Online Library for rules of use; OA articles are governed by the applicable Creative Commons License

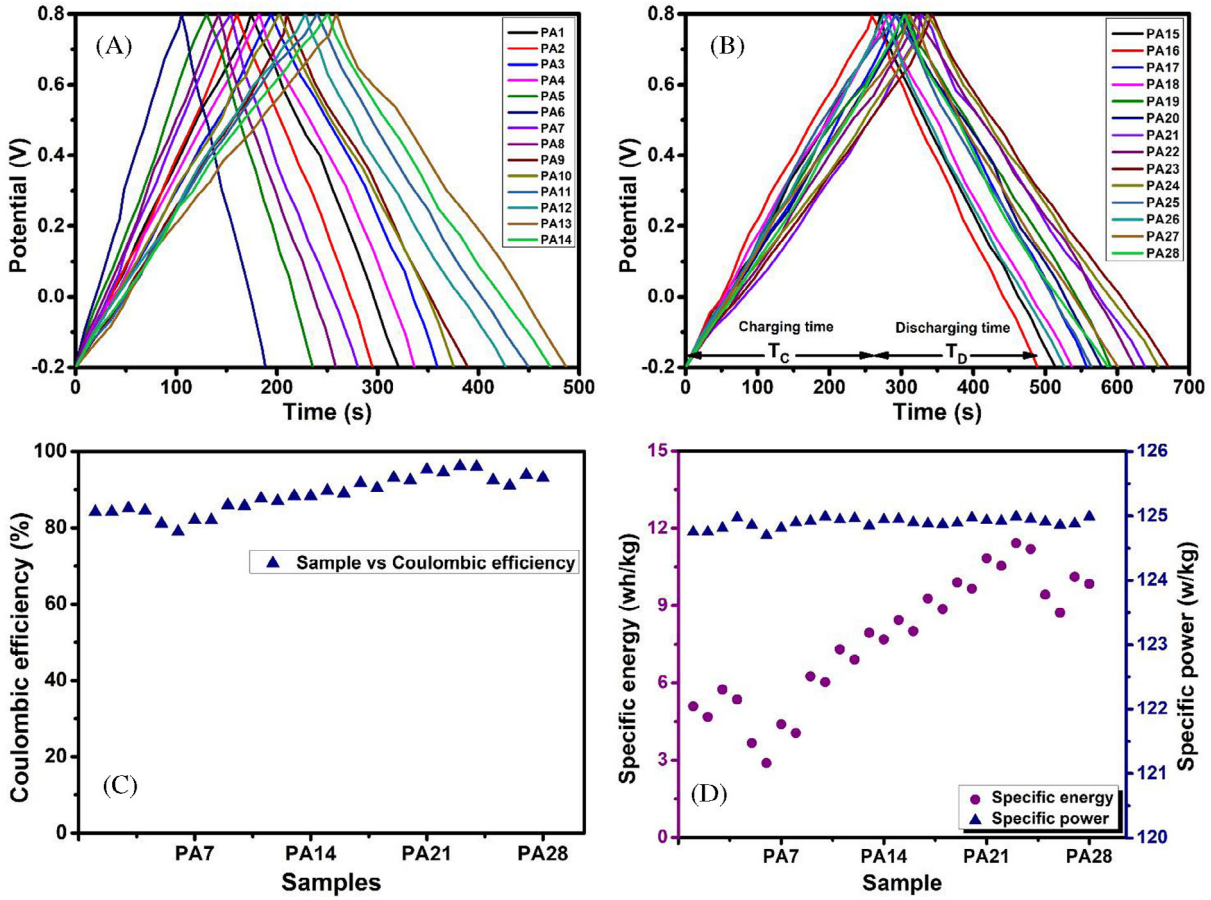

FIGURE 3 (A and B) Charging-discharging behavior, (C) coulombic efficiency, and (D) Ragone plot in 2E configuration

(triangular) plateaus and the linearity resembles excellent electrochemical reversibility. During the discharging process no potential or IR drop was observed, which suggests very less loss of the internal energy during probable electrochemical reactions. This suggests that the systems have low internal resistances; so, during the CD process less energy is wasted which truncate the generation of unwanted heat.[17,18] In case of all the PANI samples, the charging-discharging curves are almost symmetric. But they show different specific capacitances, which could be attributed to the presence of oligomers due to incomplete polymerization at inappropriate ratio of APS:aniline or aniline:PTSA.

Equation (3) is used to calculate the specific capacitance from CD plots.

$$C_{SC,2E} = \frac{I \times TD}{MT \times \Delta V}, \tag{3}$$

where I and T_D are the discharging current (mA) and discharging time (s), respectively. The specific capacitance obtained from CD data is the highest for PA23 and the lowest for PA6, that is, 82.22 and 20.78 F/g, respectively.

In case of supercapacitors, the specific capacitances decrease with the increase in scan rate and current. Figure S13 shows the CV plots at different scan rates of 50 and 100 mV/s. From Table S1, it can be seen that the specific capacitance is decreasing with the increase in scan rate. Similarly, at higher current the specific capacitance decreases and the corresponding graphs have been provided in Figure S14. At higher scan rate and current, the electrolyte ions do not get enough time to react with the redox species; so, they could not underdo desirable redox transitions which directly put negative effect on the electrochemical performances of the systems (decreased capacitance). Since, energy density is directly proportional to the specific capacitance of the system, we get less energy density at higher current.

Figure S15 gives an idea about the change in EDLC and pseudocapacitance contribution with the change in scan rate. It can be observed that with the increase in scan rate, the EDLC contribution increases as the desirable redox transitions could not happen at higher scan rate due to the less residence time of the electrolyte ions at the active sites.

10991145, 2022, 14, Downloaded from https://onlinelibrary.wiley.com/doi/10.1002/er.8690 by Indian Institute Of Technology, Wiley Online Library on [18/04/2023]. See the Terms and Conditions (https://onlinelibrary.wiley.com/terms-and-conditions) on Wiley Online Library for rules of use; OA articles are governed by the applicable Creative Commons License

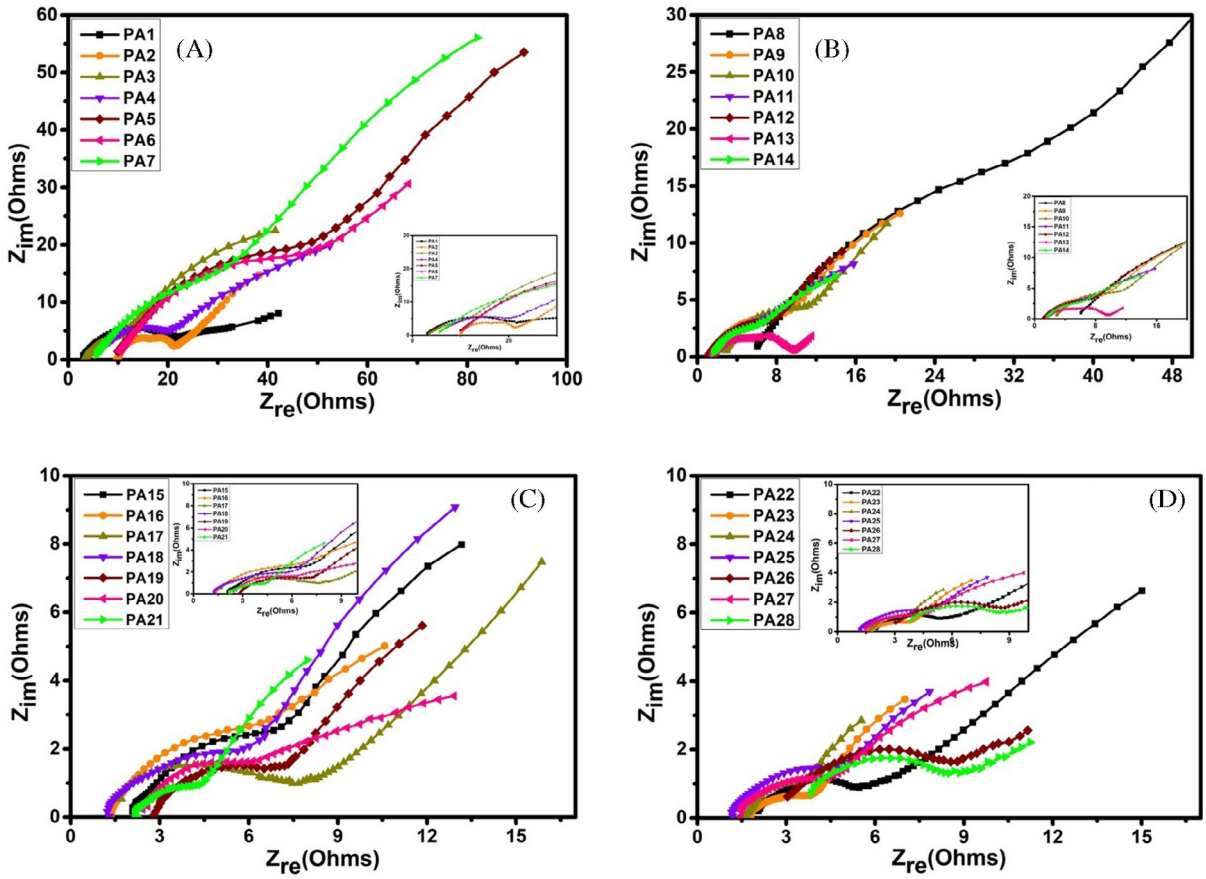

FIGURE 4 EIS plots of all the electrodes

From the charging and discharging time we have calculated the coulombic efficiencies (CEs) of the devices (Equation 4). Coulombic (Faradaic) efficiency resembles the efficiency with which electrons (charges) are transferred in a device to facilitate the desired electrochemical reactions. From Figure 3C we can see that PA23 has the highest CE of 95.95% and PA6 has the lowest CE of 78.93%. From T_D (discharging time) and T_C (charging time), the CE was calculated.

$$\eta(\%) = \frac{TD}{TC} \times 100. \tag{4}$$

For practical applications, measurement of specific energy (S_E) and power (S_P) are necessary. Specific energy is the efficiency of a device to store charge and specific power represents its quickness to deliver the stored charge. Equations (5) and (6) are used to calculate the S_E and S_P of the device. PA23 has the highest S_P and S_E of 124.99 W/kg and 11.42 Wh/kg, respectively (Figure 3D).

$$S_E = \frac{1}{2} C_{SC,2E} V^2, \tag{5}$$

$$S_P = \frac{S_E}{T_D}, \tag{6}$$

where S_E is specific energy (Wh/kg) and S_P is specific power (W/kg).

During charging and discharging process of these conducting polymers, the polymer backbones undergo immense stress due to continuous expansion and contraction. They must be capable of bearing the sudden change in their structure to avoid pore ruptures which could destroy their electrical connectivity and hinder the proper tunnelling of electrolyte ions to the electro active sites.[19,20] In the FESEM micrographs, we can observe that the PA23 sample has a more uniform surface morphology than the other samples. Due to the uniformity, electrolyte ions must be getting proper channels for the smooth movement through the interior of the active material, which could be the probable reason for better capacitance, CE, specific power, specific energy in case of PA23. PA23 has APS to aniline ratio of 1.25:1 and aniline to PTSA ratio of 2:1; these proportions of the constituents must be avoiding the formation of unwanted oligomers

1099114x, 2022, 14, Downloaded from https://onlinelibrary.wiley.com/doi/10.1002/er.8690 by Indian Institute Of Technology, Wiley Online Library on [18/04/2023]. See the Terms and Conditions (https://onlinelibrary.wiley.com/terms-and-conditions) on Wiley Online Library for rules of use; OA articles are governed by the applicable Creative Commons License

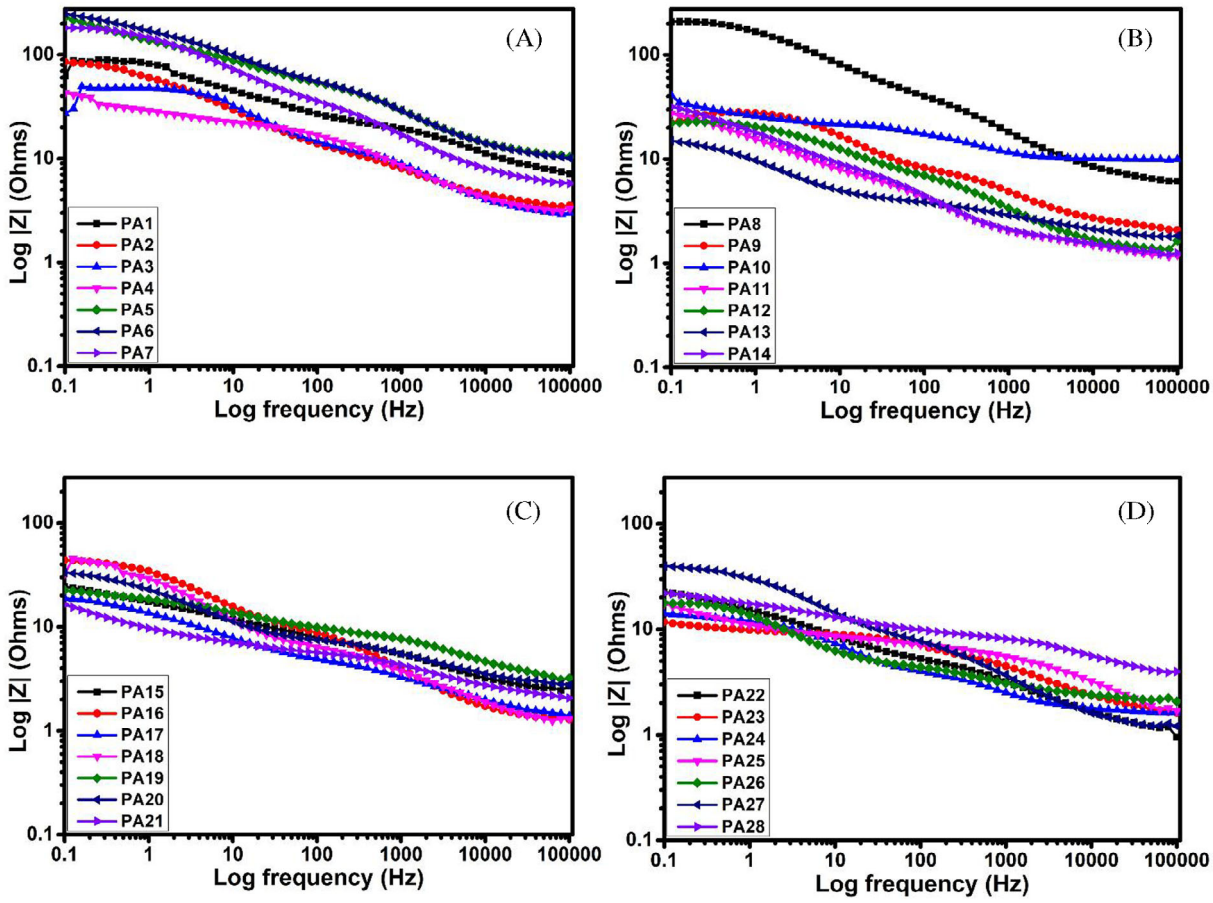

FIGURE 5 Frequency vs |*Z*| plots

and favoring complete polymerization with outstanding uniformity.[21,22] The unvarying and regular structure can withstand any abrupt change in the polymer backbone and could provide better stability to the system.

EIS was carried out for the evaluation of the impedances of the electrodes (Figure 4). The real part in EIS plot demonstrates the resistive behavior and imaginary part resembles capacitive nature of the system. The first intercept of the quasi semicircle in the real *Z*-axis is the equivalent series resistance (R_S), which is the combination of resistances coming from current collector, substrate, electrolyte, and so forth. Diameter of the semicircle resembles the charge transfer resistance (R_{CT}) of the electrode, which is the contribution of interfacial and bulk resistances, and normally observed at higher frequency region. The steep line in the low frequency region is the signature of Warburg resistance, which is generated due to the interruptions caused during diffusion process because of abrupt uniformity and porosity of the samples.[23,24] PA23 has the least charge transfer resistance of 3.1 Ω and PA6 has the largest R_{CT} of 79.2 Ω. When electrodes are immersed in the electrolyte (KOH), the ions start migrating from the bulk solution to the electro active sites of the materials. Materials with uniform structure favor easy tunnelling of the electrolyte ions and they (ions) get less resistance during the diffusion process. The inset in Figure 4D represents the equivalent circuit (EC) that fits to our systems. We have simulated the EIS data in ZSimpWin to fit them with probable equivalent electrical circuit (EEC) and they have been given in Figure S3. The EEC has two capacitive elements, one constant phase element (CPE), and four resistive elements. R_S is the combined resistances coming from the electrolyte, current collector, and substrate. C_{DL} and R_{CT} are in parallel combination, where C_{DL} is the EDLC and R_{CT} is the charge transfer resistance.[16,25] All the systems are deviating from the ideal capacitor behavior as the plots in the lower frequency regions are not parallel to the *Z*-imaginary axis. So, a CPE, *Q* has been introduced in the EC. The resistive element associated to the CPE arises from the diffusion process, which takes place at the interface of the porous electrode-electrolyte. Electrode materials having nonuniform pore dimensions create such kind of diffusion resistances. The straight line in the low frequency region signifies ideal polarizable capacitance known as the mass

10991145x, 2022, 14, Downloaded from https://onlinelibrary.wiley.com/doi/10.1002/er.8690 by Indian Institute Of Technology, Wiley Online Library on [18/04/2023]. See the Terms and Conditions (https://onlinelibrary.wiley.com/terms-and-conditions) on Wiley Online Library for rules of use; OA articles are governed by the applicable Creative Commons License

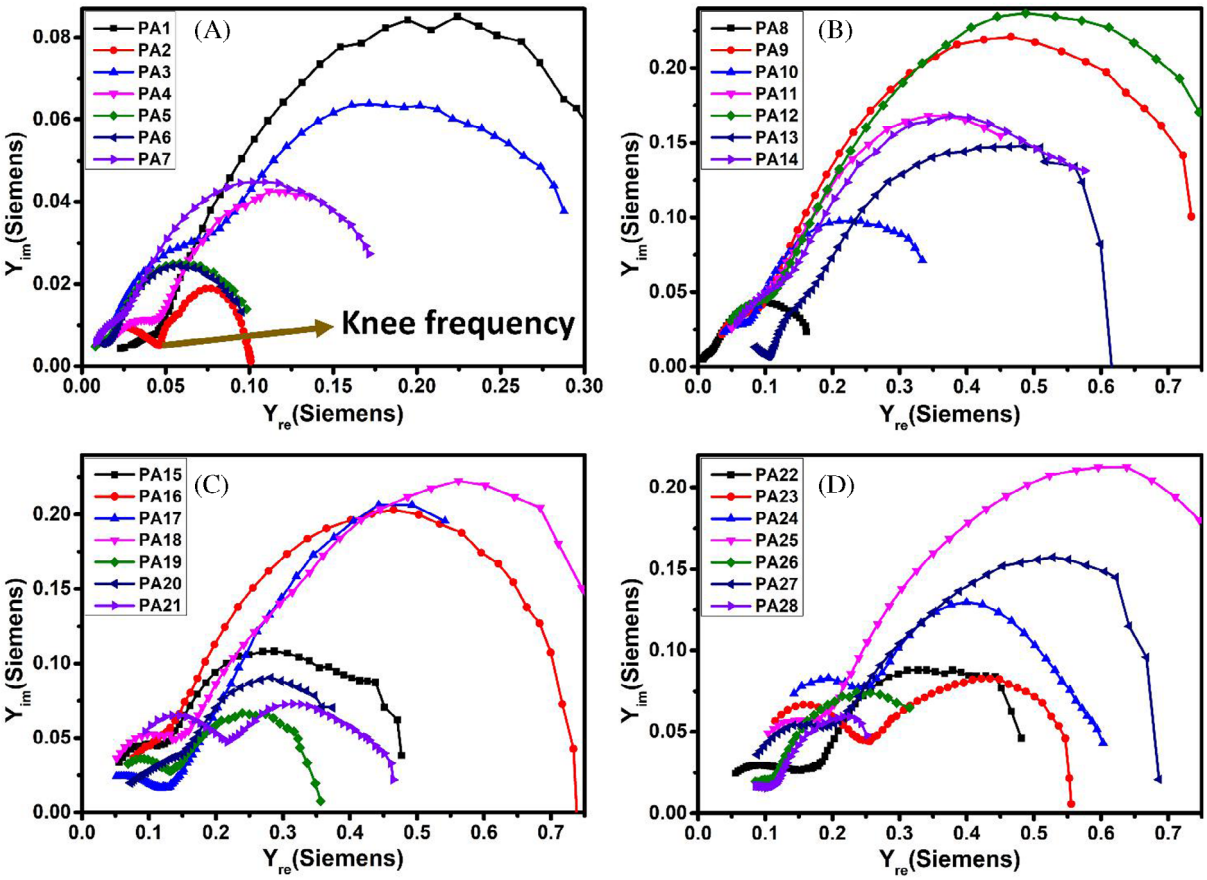

FIGURE 6 Admittance plot

capacitance (C_L). But the inclination of this line suggests that C_L is associated to a resistance, which is called as leakage resistance (R_L).[15,26]

From Figure 5 we can see that the total impedance of all the systems are maximum at low frequency, they decrease with the increase in frequency, and become almost constant at high frequency. At lower frequencies, the electrolyte ions tend to migrate from the electrode surface to the porous texture of the electrodes. These pores contribute to the capacitive and resistive nature resulting a higher impedance. On contrary to this, at higher frequencies, the electrolyte ions may be limited till the surface or just penetrate through the opening of the pores, creating less impedance.[27,28] PA23 has the least net impedance of 11.6 Ω at the low frequency region and PA6 has the highest net impedance of 248 Ω at the respective region. This suggests that the migration of electrolyte ions offer less hindrance in case of PA23.

The admittance plot has a knee, which is the transition point between high frequency and low frequency region. The knee frequency (f_k) represents the maximum value of frequency at which capacitive nature is dominating, and it resembles the power performances of supercapacitors. In other words, we can say that knee frequency is the upper limit below which capacitive nature can be regulated properly and the stored energy can be fully accessed.[29,30] Therefore, a higher value of f_k is always desirable. Knee frequencies of the samples are obtained from the admittance plot (Figure 6A-D), and Table 2 contains values of f_k and the corresponding relaxation time (τ_r). On the basis of specific capacitance obtained from CV and CD, CE, specific energy, specific power, charge transfer resistance PA23 has been found out to be the best sample. So, we have taken three best and two worst sample into consideration for the knee frequency study. PA23 and PA6 have the highest and the lowest f_k of 251 and 50 Hz, respectively. The corresponding relaxation time for PA23 and PA6 are 4 and 20 ms, respectively. These data indicate that for PA23 the stored energy can be accessed effectively till 251 Hz and for PA6 as high as 50 Hz. Lower knee frequency indicates higher charge transfer resistance. In the Nyquist plot (Figure 4A), we found that PA6 had the highest charge transfer resistance of 79.2 Ω; so, it is logically justified if we are getting lower knee frequency for PA6. Similarly, lower relaxation time of PA23 indicates that it can show capacitive nature more quickly than other samples.

10991145x, 2022, 14, Downloaded from https://onlinelibrary.wiley.com/doi/10.1002/er.8690 by Indian Institute Of Technology, Wiley Online Library on [18/04/2023]. See the Terms and Conditions (https://onlinelibrary.wiley.com/terms-and-conditions) on Wiley Online Library for rules of use; OA articles are governed by the applicable Creative Commons License

TABLE 2 Various values obtained from the electrochemical testing for the best three and the worst two systems

Sample	$\|Z\|$ at low frequency (Ω)	Knee frequency (Hz)	Relaxation time (ms)	R_{CT} (Ω)
PA5	227	79	12.6	69
PA6	248	50	20	79.2
PA21	16.4	125	8	3.9
PA23	11.6	251	4	3.1
PA24	14	159	6.3	3.6

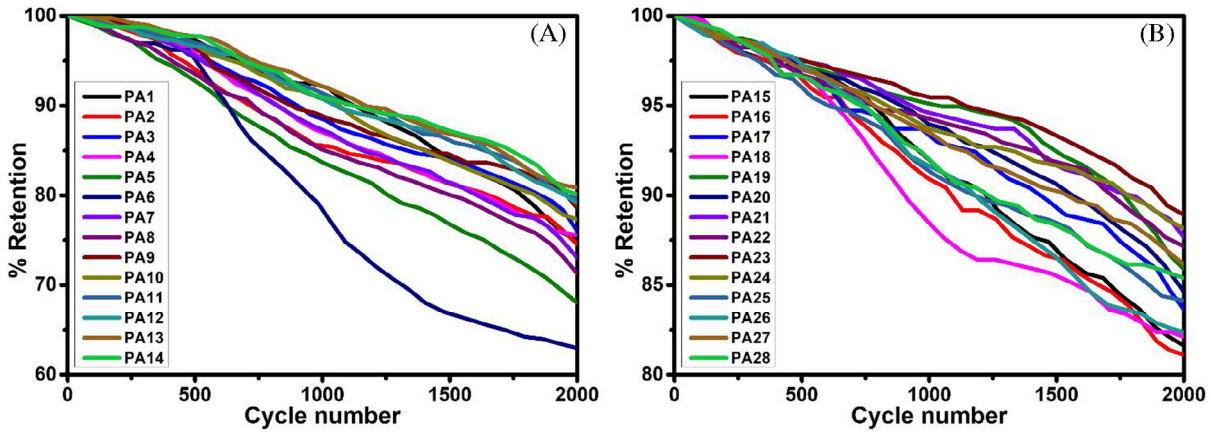

FIGURE 7 Cycle life after 2000 cycles

Figure S4 represents the frequency vs admittance ($|Y|$) plot of PA5, PA6, PA21, PA23, and PA24. All the electrodes have low admittance in the low frequency part and increased with rise in frequency. At the low frequency, more charges accumulated at the electrode-electrolyte interface leading to the diminution of mobile ions, and the admittance decreased. However, at higher frequency, the mobility of ions (charge carriers) increased and therefore, the admittance also increased with increase in frequency.[15,26]

CV of the fabricated electrodes was carried out at 200 mV/s for 2000 cycles to evaluate their percentage capacitance retention (Figure 7). During the charging and discharging process, the polymer backbone experiences tremendous expansion and contraction, which degrade the cycle life of the corresponding electrode. Complete polymerization and perfect crosslinking could help the polymer backbone to withstand the abrupt volumetric changes by providing a robust structure and could potentially prevent the polymer degradation.[15,31] PA23 has the highest capacitance retention of 88.97% and PA6 has the lowest retention of 62.97% after 2000 cycles. So, we can propose that the ratio of APS:aniline and aniline: PTSA taken for PANI synthesis are optimized for PA23 on the basis of electrochemical characterizations.

In Table 3 we have provided a brief comparison between the systems fabricated by us and the previously studied PANI-based systems. Multiple parameters like specific capacitance, power density, energy density, CE, charge transfer resistance, CE, and so forth are taken to decide the best material for energy storage.

3.2 | Material characterization

3.2.1 | Morphological analysis

During the polymerization reaction, PTSA plays the role of dopant as well as surfactant. PTSA forms micelles in aqueous solution due to the existence of hydrophilic and hydrophobic groups like $-SO_3H$. When we add aniline to PTSA solution, a complex is formed due to the interaction between $-NH_2$ group of aniline and $-SO_3H$ group of PTSA, and the complex acts as the nucleation site for the growth of PANI having different structures.[47] During the oxidative polymerization of aniline, when we add APS, it turns to PANI EB which does not contain any charged molecule and the molecules form aggregates. After adding desired amount of APS, EB gets converted to ES and two different cases may arise. Case 1: Cationic nature of PANI ES prevents the molecules to aggregate due to electrostatic repulsion between them. Case 2: Formation of excessive oligomers, incomplete polymerization, and partial doping of PANI ES could create aggregation due to

1099114x, 2022, 14, Downloaded from https://onlinelibrary.wiley.com/doi/10.1002/er.8690 by Indian Institute Of Technology, Wiley Online Library on [18/04/2023]. See the Terms and Conditions (https://onlinelibrary.wiley.com/terms-and-conditions) on Wiley Online Library for rules of use; OA articles are governed by the applicable Creative Commons License

TABLE 3 Information about few conducting polymer-based supercapacitor electrodes and their electrochemical properties

Material	C_{SP} (F/g)	ν or A_ρ	Cycle life	Reference
PANI Nanosheet	272	1 A/g	50% (3000)	32
PANI Nanorod	286.7	1 mV/s	41% (1300)	33
PANI-SA Hydrogel	252	0.5 A/g	71% (1000)	34
PANI Aerogel	184	0.5 A/g	74% (1000)	35
PANI-HCl	70	1.25 mA/cm^2	57% (1000)	36
PANI on CNF	264	5 mV/s	NR	30
PANI-$LiPF_6$	80	2 mA/cm^2	75% (5000)	37
PANI/Fe_3O_4	213	1 mA/cm^2	NR	38
PPY-SWNTs	144	200 mV/s	NR	39
PEDOT on PPY	230	2 mV/s	95% (1000)	29
AC/PANI	273	50 mV/s	NR	40
PEDOT	100	5 mV/s	80% (5000)	41
MWNT/PANI	360	5 mV/s	92% (1000)	42
PANI-CNF	264	5 mV/s	NR	30
PANI-NFs	267	0.35 A/g	86% (1000)	43
PANI-AB	132	0.3 A/g	91% (100)	44
PANI-CNT	144	5 mV/s	92.3% (200)	45
PANI-Bamboo	244	0.5 A/g	92% (1000)	46
PTSA based PANI	301.49	5 mV/s	88.97% (2000)	Present work

the attraction between undoped sites.[48] Figure S5 demonstrates the FESEM images of PA5, PA6, PA21, PA23, and PA24. In PA5 and PA6, we can see that the particles of PANI have been agglomerated. The large extent of agglomeration must be obstructing the seamless movement of electrolyte ions to the active sites; therefore, these samples exhibit inferior electrochemical properties. PA23 is consisting of uniform structures, which must be providing better electrical connection during the electrochemical activities, thereby exhibiting enormous electrochemical properties. PA24 possess rod like structures along with few agglomerations. PA21 has agglomerated structures along with threads connecting the agglomerated large particles. At PANI:PTSA ratio of 2:1 and APS: aniline ratio of 1.25:1, there might be less oligomers present in the material; thereby, prohibiting any agglomeration which provides more uniformity than other samples. The ordered structure could be driving the electrochemical performances in case of PA23. From EDS (Figure S6), we confirm successful doping of sulfur in PANI. In PA5, PA6, PA21 the amounts of PTSA are higher compared to PA23 and PA24. From the electrochemical testing we exhibited that PA23 has the best electrochemical properties. So, it must be kept in mind that an optimized level of doping is required for outstanding electrochemical performances. The elemental mapping has been given in Figure S7 and it shows that PA5, PA6, and PA21 has more sulfur than PA23 and PA24 at a particular region, which justifies the EDS results and the proportion we have taken during material preparation. TEM plots of PA23 have been given in Figure S8. The HR image shows agglomeration of rod and some irregular shaped structures. The SAED pattern exhibits diffused rings, which could be due to the broad diffraction pattern of PANI.

Figure S9 shows the 2D (a) and 3D (b) surface roughness, 2D grain boundary (c) obtained from AFM analysis for PA23. The root mean square and average roughness were found to be 162 and 126 nm, respectively. This roughness would have arisen due to the grain formation and porosity of PANI. Roughness and cracks play a vital role in the movement and trapping of electrolyte ions during the electrochemical processes, which help in accessing more active surface area.[49,50] It must be noted that the roughness parameters were captured from scanning area of $60 \times 60\ \mu m^2$, and they may give different results depending upon the scan area.

3.2.2 | Rheological study

Figure S10 represents the rheological behavior of PA23. In general, a coating can last longer if the material

10991145, 2022, 14, Downloaded from https://onlinelibrary.wiley.com/doi/10.1002/er.8690 by Indian Institute Of Technology, Wiley Online Library on [18/04/2023]. See the Terms and Conditions (https://onlinelibrary.wiley.com/terms-and-conditions) on Wiley Online Library for rules of use; OA articles are governed by the applicable Creative Commons License

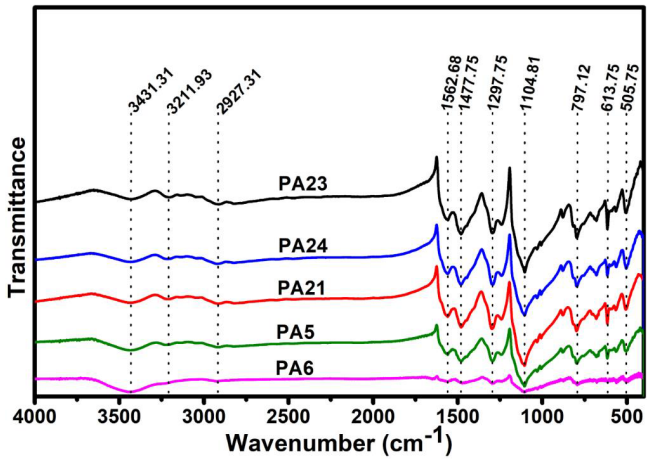

FIGURE 8 FTIR of PA5, PA6, PA21, PA23, PA24

exhibits non-Newtonian behavior, that is, dependant on the shear rate. It can be seen that the viscosity is decreasing with increase in shear rate till 10 s^{-1}, that is, PA23 exhibited shear thinning property in that range. After 10 s^{-1}, shear rate has no effect on the viscosity. The shear thinning property of PA23 could help it to stick to the substrate for a longer time, thereby enhancing the cycle life.[51]

3.2.3 | X-ray diffraction

From all the electrochemical characterizations, we found that PA5, PA6 showed inferior electrochemical properties and PA21, PA23, PA24 exhibited excellent activity. So, we performed XRD of all the above-mentioned samples to find out their crystalline nature (Figure S11). In literature, it has been reported that PANI exhibit semicrystalline nature, which could be due to the chain folding of PANI chains in a systematic manner.[52] The low crystallinity of PANI could be due to the presence of repeated quinoid and benzenoid rings in the PANI chain.[53] All the samples have almost same diffraction patterns and the peaks are positioned at 14.79°, 20.33°, 25.22°. The peak at 20.33° and 25.22° could be due to the parallel and perpendicular periodicity to the conducting PANI chains. The characteristic peaks at 20.33° and 25.22° are because of (020) and (200) planes of PANI. The diffraction peak at 14.79° is due to the existence of (011) plane. Scherrer's formula (Equation 7) is used to calculate the average crystallite size, and the estimated crystallite sizes of PA5, PA6, PA21, PA23, and PA24 are 3.1, 3.32, 1.48, 1.32, and 1.46 nm, respectively. In general, materials having smaller crystallite sizes offer more active sites for electrochemical reactions due to higher dislocation density along with broader grain boundary.[54]

$$D = \frac{S\lambda}{\beta\cos\theta}, \tag{7}$$

where D is crystallite size (nm); λ is the wavelength (1.54 Å); S is the shape factor (0.94); β is the full-width at half maxima (in radians); and θ is Bragg's angle.

3.2.4 | Fourier transform infrared

FTIR was done to identify the existing functional groups in the samples, and Figure 8 represents the corresponding information. Transmittance at 505.75 cm^{-1} could be due to the C–Br bond as KBr was taken as a binder while preparing pellets. The spectrum at 613.75 cm^{-1} could be due to the unsymmetric stretching of S–O groups in PANI-PTSA.[55] Peak at 797.12 cm^{-1} could have been due to –CH deformation. A broad spectrum at 1104.81 cm^{-1} resembles stretching vibration of –N═Q═N–. Transmittance at 1297.75 cm^{-1} could have happened due to the stretching of C–N and C–N^+, which could be linked to protonation during the polymerization process of PANI. Transmittance at 1562.68 and 1477.75 cm^{-1} are ascribed to quinoid and benzenoid ring stretching vibrations, respectively. NH and NH_2^+ groups present in PANI produce stretching vibrations at wavenumbers of 2927.31 and 3431.31 cm^{-1}. The –OH stretching vibration would have created the transmittance spectrum at 3211.93 cm^{-1}.[17,56]

4 | CONCLUSION

We have successfully synthesized PTSA-based conducting PANI for supercapacitor electrode applications. The primary aim was to find out the optimized ratio of APS:aniline and aniline:PTSA based on the electrochemical performances of the fabricated electrodes. PA23 exhibited excellent electrochemical properties, which has APS:aniline ratio of 1.25:1 and aniline:PTSA ratio of 2:1. PA23-based supercapacitor has the highest value of specific capacitance, specific energy, specific power, and CE of 82.22 F/g, 11.42 Wh/kg, 124.99 W/kg, and 95.95%, respectively. It offers very low charge transfer resistance of 3.1 Ω during the electrochemical processes. The cycle life of PA23-based system is the largest among all, which is 88.97% retention after 2000 cycles. The robust electrochemical behavior could be due to the uniform rod-shaped morphology of the corresponding system, which might be providing seamless movement of the electrolyte ions to the electrochemical active sites along with proper electrical connection. So, PA23 based sample has the optimized proportion of the constituents. It can be

1099114x, 2022, 14, Downloaded from https://onlinelibrary.wiley.com/doi/10.1002/er.8690 by Indian Institute Of Technology, Wiley Online Library on [18/04/2023]. See the Terms and Conditions (https://onlinelibrary.wiley.com/terms-and-conditions) on Wiley Online Library for rules of use; OA articles are governed by the applicable Creative Commons License

proposed that APS:aniline has more contribution than aniline:PTSA as APS works as an initiator for the polymerization of aniline.

ACKNOWLEDGMENT

The author, Tapas Das, is grateful to the Ministry of Human Resource Development, India (MHRD, India) for giving required financial support and the Indian Institute of Technology BHU, Varanasi (IIT BHU) for providing all the facilities to accomplish the research goal.

DATA AVAILABILITY STATEMENT

Data sharing is not applicable to this article as no new data were created or analyzed in this study.

REFERENCES

1. Grover S, Goel S, Marichi RB, Sahu V, Singh G, Sharma RK. Polyaniline all solid-state pseudocapacitor: role of morphological variations in performance evolution. *Electrochim Acta*. 2016;196:131-139. doi:10.1016/j.electacta.2016.02.157
2. Grover S, Goel S, Sahu V, Singh G, Sharma RK. Asymmetric supercapacitive characteristics of PANI embedded holey graphene nanoribbons. *ACS Sustainable Chem Eng*. 2015;3(7):1460-1469. doi:10.1021/acssuschemeng.5b00184
3. Han J, Dai J, Zhou C, Guo R. Dilute cationic surfactant-assisted synthesis of polyaniline nanotubes and application as reactive support for various noble metal nanocatalysts. *Polym Chem*. 2013;4(2):313-321. doi:10.1039/c2py20536j
4. Wang H, Liu J, Chen Z, et al. Synergistic capacitive behavior between polyaniline and carbon black. *Electrochim Acta*. 2017;230:236-244. doi:10.1016/j.electacta.2017.01.164
5. Silva CHB, Galiote NA, Huguenin F, Teixeira-Neto É, Constantino VRL, Temperini MLA. Spectroscopic, morphological and electrochromic characterization of layer-by-layer hybrid films of polyaniline and hexaniobate nanoscrolls. *J Mater Chem*. 2012;22(28):14052-14060. doi:10.1039/c2jm31531a
6. Banerjee J, Dutta K, Kader MA, Nayak SK. An overview on the recent developments in polyaniline-based supercapacitors. *Polym Adv Technol*. 2019;30(8):1902-1921. doi:10.1002/pat.4624
7. Çolak N, Sükmen B. Doping of chemically synthesized polyaniline. *Des Monomers Polym*. 2000;3(2):181-189. doi:10.1163/156855500300142870
8. Simotwo SK, Kalra V. Polyaniline-based electrodes: recent application in supercapacitors and next generation rechargeable batteries. *Curr Opin Chem Eng*. 2016;13:150-160. doi:10.1016/j.coche.2016.09.001
9. MacDiarmid AG, Epstein AJ. Polyanilines: a novel class of conducting polymers. *Faraday Discuss Chem Soc*. 1989;88:317-332. doi:10.1039/DC9898800317
10. Park HW, Kim T, Huh J, Kang M, Lee JE, Yoon H. Anisotropic growth control of polyaniline nanostructures and their morphology-dependent electrochemical characteristics. *ACS Nano*. 2012;6(9):7624-7633. doi:10.1021/nn3033425
11. Chen W, Rakhi RB, Alshareef HN. Morphology-dependent enhancement of the pseudocapacitance of template-guided tunable polyaniline nanostructures. *J Phys Chem C*. 2013;117(29):15009-15019. doi:10.1021/jp405300p
12. Bláha M, Varga M, Prokeš J, Zhigunov A, Vohlídal J. Effects of the polymerization temperature on the structure, morphology and conductivity of polyaniline prepared with ammonium peroxodisulfate. *Eur Polym J*. 2013;49(12):3904-3911. doi:10.1016/j.eurpolymj.2013.08.018
13. Maity PC, Khandelwal M. Synthesis time and temperature effect on polyaniline morphology and conductivity. *Am J Mater Synth Process*. 2016;1(4):37-42. doi:10.11648/j.ajmsp.20160104.11
14. Niziol J, Sniechowski M, Podraza-Guba A, Pielichowski J. Alternative oxidizers in polyaniline synthesis. *Polym Bull*. 2011;66(6):761-770. doi:10.1007/s00289-010-0309-7
15. Kausar A. High-performance competence of polyaniline-based nanomaterials. *Mater Res Innov*. 2020;24(2):113-122. doi:10.1080/14328917.2019.1611253
16. Yu H, Lv R, Wu H, Qian C, Wang S, Chen M. Fabrication of ternary hierarchical nanosheets RGO/PANI/Fe_2O_3 as electrode material with high capacitance performance. *J Electrochem Soc*. 2020;167(4):040501. doi:10.1149/1945-7111/ab6dd4
17. Xu Z, Wang T, Wang L, et al. Aniline-grafting graphene oxide/polyaniline composite prepared via interfacial polymerization with high capacitive performance. *Int J Energy Res*. 2019;43(13):7693-7701. doi:10.1002/er.4756
18. Prasanna BP, Avadhani DN, Chaitra K, Nagaraju N, Kathyayini N. Synthesis of polyaniline/MWCNTs by interfacial polymerization for superior hybrid supercapacitance performance. *J Polym Res*. 2018;25:123. doi:10.1007/s10965-018-1526-2
19. Aparna ML, Grace AN, Sathyanarayanan P, Sahu NK. A comparative study on the supercapacitive behaviour of solvothermally prepared metal ferrite (MFe_2O_4, M = Fe, Co, Ni, Mn, Cu, Zn) nanoassemblies. *J Alloys Compd*. 2018;745:385-395. doi:10.1016/j.jallcom.2018.02.127
20. Mezgebe MM, Yan Z, Wei G, et al. 3D graphene-Fe_3O_4-polyaniline, a novel ternary composite for supercapacitor electrodes with improved electrochemical properties. *Mater Today Energy*. 2017;5:164-172. doi:10.1016/j.mtener.2017.06.007
21. Akhtar MA, Sharma V, Biswas S, Chandra A. Tuning porous nanostructures of $MnCo_2O_4$ for application in supercapacitors and catalysis. *RSC Adv*. 2016;6(98):96296-96305. doi:10.1039/c6ra20004d
22. Dubal DP, Ayyad O, Ruiz V, Gómez-Romero P. Hybrid energy storage: the merging of battery and supercapacitor chemistries. *Chem Soc Rev*. 2015;44(7):1777-1790. doi:10.1039/c4cs00266k
23. Zhang Q, Wang N, Zhao P, Yao M, Hu W. Azide-assisted hydrothermal synthesis of N-doped mesoporous carbon cloth for high-performance symmetric supercapacitor employing $LiClO_4$ as electrolyte. *Compos Part A Appl Sci Manuf*. 2017;98:58-65. doi:10.1016/j.compositesa.2017.03.013
24. Asen P, Shahrokhian S, Iraji zad A. Ternary nanostructures of Cr_2O_3/graphene oxide/conducting polymers for supercapacitor application. *J Electroanal Chem*. 2018;823:505-516. doi:10.1016/j.jelechem.2018.06.048
25. Noremberg BS, Silva RM, Paniz OG, et al. From banana stem to conductive paper: a capacitive electrode and gas sensor. *Sens Actuators B*. 2017;240:459-467. doi:10.1016/j.snb.2016.09.014

1099114x, 2022, 14, Downloaded from https://onlinelibrary.wiley.com/doi/10.1002/er.8690 by Indian Institute Of Technology, Wiley Online Library on [18/04/2023]. See the Terms and Conditions (https://onlinelibrary.wiley.com/terms-and-conditions) on Wiley Online Library for rules of use; OA articles are governed by the applicable Creative Commons License

26. Nabi G, Raza W, Kamran MA, et al. Role of cerium-doping in $CoFe_2O_4$ electrodes for high performance supercapacitors. *J Energy Storage*. 2020;29:101452. doi:10.1016/j.est.2020.101452
27. Liao F, Han X, Zhang Y, Han X, Xu C, Chen H. Hydrothermal synthesis of mesoporous $MnCo_2O_4/CoCo_2O_4$ ellipsoid-like microstructures for high-performance electrochemical supercapacitors. *Ceram Int*. 2019;45(6):7244-7252. doi:10.1016/j.ceramint.2019.01.005
28. Qiu Z, Peng Y, He D, Wang Y, Chen S. Ternary Fe_3O_4@C@-PANi nanocomposites as high-performance supercapacitor electrode materials. *J Mater Sci*. 2018;53(17):12322-12333. doi:10.1007/s10853-018-2451-9
29. Wang J, Xu Y, Chen X, Du X. Electrochemical supercapacitor electrode material based on poly(3,4-ethylenedioxythiophene)/polypyrrole composite. *J Power Sources*. 2007;163(2):1120-1125. doi:10.1016/j.jpowsour.2006.10.004
30. Jang J, Bae J, Choi M, Yoon SH. Fabrication and characterization of polyaniline coated carbon nanofiber for supercapacitor. *Carbon*. 2005;43(13):2730-2736. doi:10.1016/j.carbon.2005.05.039
31. Nanofiber GP, Wu Q, Xu Y, Yao Z, Liu A, Shi G. Supercapacitors based on flexible graphene/polyaniline nanofiber composite films. *ACS Nano*. 2010;4(4):1963-1970. doi:10.1021/nn1000035
32. Xie F, Zhou M, Wang G, Wang Q, Yan M, Bi H. Morphology-dependent electrochemical performance of nitrogen-doped carbon dots@polyaniline hybrids for supercapacitors. *Int J Energy Res*. 2019;43(3):7529-7540. doi:10.1002/er.4678
33. Wang X, Deng J, Duan X, Liu D, Guo J, Liu P. Crosslinked polyaniline nanorods with improved electrochemical performance as electrode material for supercapacitors. *J Mater Chem A*. 2014;2(31):12323-12329. doi:10.1039/c4ta02231a
34. Huang H, Zeng X, Li W, Wang H, Wang Q, Yang Y. Reinforced conducting hydrogels prepared from the in situ polymerization of aniline in an aqueous solution of sodium alginate. *J Mater Chem A*. 2014;2(39):16516-16522. doi:10.1039/c4ta03332a
35. Zhao HB, Yuan L, Fu ZB, et al. Biomass-based mechanically strong and electrically conductive polymer aerogels and their application for supercapacitors. *ACS Appl Mater Interfaces*. 2016;8(15):9917-9924. doi:10.1021/acsami.6b00510
36. Ryu KS, Kim KM, Park NG, Park YJ, Chang SH. Symmetric redox supercapacitor with conducting polyaniline electrodes. *J Power Sources*. 2002;103(2):305-309. doi:10.1016/S0378-7753(01)00862-X
37. Ryu KS, Kim KM, Park YJ, Park NG, Kang MG, Chang SH. Redox supercapacitor using polyaniline doped with Li salt as electrode. *Solid State Ion*. 2002;152-153:861-866. doi:10.1016/S0167-2738(02)00386-7
38. Radhakrishnan S, Prakash S, Rao CRK, Vijayan M. Organically soluble bifunctional polyaniline-magnetite composites for sensing and supercapacitor applications. *Electrochem Solid St*. 2009;12(4):84-87. doi:10.1149/1.3074315
39. Wang J, Xu Y, Chen X, Sun X. Capacitance properties of single wall carbon nanotube/polypyrrole composite films. *Compos Sci Technol*. 2007;67(14):2981-2985. doi:10.1016/j.compscitech.2007.05.015
40. Ryu KS, Lee YG, Kim KM, et al. Electrochemical capacitor with chemically polymerized conducting polymer based on activated carbon as hybrid electrodes. *Synth Met*. 2005;153(1–3):89-92. doi:10.1016/j.synthmet.2005.07.167
41. Li W, Chen J, Zhao J, Zhang J, Zhu J. Application of ultrasonic irradiation in preparing conducting polymer as active materials for supercapacitor. *Mater Lett*. 2005;59(7):800-803. doi:10.1016/j.matlet.2004.11.024
42. Khomenko V, Frackowiak E, Béguin F. Determination of the specific capacitance of conducting polymer/nanotubes composite electrodes using different cell configurations. *Electrochim Acta*. 2005;50(12):2499-2506. doi:10.1016/j.electacta.2004.10.078
43. Chaudhari S, Sharma Y, Archana PS, et al. Electrospun polyaniline nanofibers web electrodes for supercapacitors. *J Appl Polym Sci*. 2013;129(4):1660-1668. doi:10.1002/app.38859
44. Ajit S, Palaniappan S, Gopukumar S. Polyaniline binder for functionalized acetylene black: a hybrid material for supercapacitor. *Synth Met*. 2013;180:43-48. doi:10.1016/j.synthmet.2013.07.022
45. Xie D, Jiang Q, Fu G, et al. Preparation of cotton-shaped CNT/-PANI composite and its electrochemical performances. *Rare Metals*. 2011;30:94-97. doi:10.1007/s12598-011-0246-0
46. Zhou X, Li L, Dong S, et al. A renewable bamboo carbon/polyaniline composite for a high-performance supercapacitor electrode material. *J Solid State Electrochem*. 2012;16(3):877-882. doi:10.1007/s10008-011-1435-3
47. Parveen N, Ansari MO, Han TH, Cho MH. Simple and rapid synthesis of ternary polyaniline/titanium oxide/graphene by simultaneous TiO_2 generation and aniline oxidation as hybrid materials for supercapacitor applications. *J Solid State Electrochem*. 2017;21(1):57-68. doi:10.1007/s10008-016-3310-8
48. Manigandan S, Jain A, Majumder S, Ganguly S, Kargupta K. Formation of nanorods and nanoparticles of polyaniline using Langmuir Blodgett technique: performance study for ammonia sensor. *Sens Actuators B*. 2008;133(1):187-194. doi:10.1016/j.snb.2008.02.020
49. de Araujo Dionisio N, de Oliveira Farias EA, Marques TA, et al. Layer-by-layer films based on polyaniline, titanate nanotubes, and cetyl trimethyl ammonium bromide for antifungal coatings. *J Coat Technol Res*. 2019;16(5):1253-1262. doi:10.1007/s11998-019-00199-1
50. Navale YH, Navale ST, Dhole IA, Stadler FJ, Patil VB. Specific capacitance, energy and power density coherence in electrochemically synthesized polyaniline-nickel oxide hybrid electrode. *Org Electron*. 2018;57:110-117. doi:10.1016/j.orgel.2018.02.037
51. da Silva Sirqueira A, Teodoro D, da Silva Coutinho M, da Silva Neto AS, dos Anjos Silva A, Soares BG. Rheological behavior of acrylic paint blends based on polyaniline. *Polimeros*. 2016;26(3):215-220. doi:10.1590/0104-1428.2178
52. Palsaniya S, Nemade HB, Dasmahapatra AK. Synthesis of polyaniline/graphene/MoS_2 nanocomposite for high performance supercapacitor electrode. *Polymer*. 2018;150:150-158. doi:10.1016/j.polymer.2018.07.018
53. Mostafaei A, Zolriasatein A. Synthesis and characterization of conducting polyaniline nanocomposites containing ZnO nanorods. *Prog Nat Sci Mater Int*. 2012;22(4):273-280. doi:10.1016/j.pnsc.2012.07.002

1099114x, 2022, 14, Downloaded from https://onlinelibrary.wiley.com/doi/10.1002/er.8690 by Indian Institute Of Technology, Wiley Online Library on [18/04/2023]. See the Terms and Conditions (https://onlinelibrary.wiley.com/terms-and-conditions) on Wiley Online Library for rules of use; OA articles are governed by the applicable Creative Commons License

54. Munirathinam B, Pydimukkala H, Ramaswamy N, Neelakantan L. Influence of crystallite size and surface morphology on electrochemical properties of annealed TiO_2 nanotubes. *Appl Surf Sci*. 2015;355:1245-1253. doi:10.1016/j.apsusc.2015.08.017
55. Wang H, Lin J, Shen ZX. Polyaniline (PANi) based electrode materials for energy storage and conversion. *J Sci Adv Mater Devices*. 2016;1(3):225-255. doi:10.1016/j.jsamd.2016.08.001
56. Jamadade VS, Dhawale DS, Lokhande CD. Studies on electrosynthesized leucoemeraldine, emeraldine and pernigraniline forms of polyaniline films and their supercapacitive behavior. *Synth Met*. 2010;160(9–10):955-960. doi:10.1016/j.synthmet.2010.02.007

SUPPORTING INFORMATION

Additional supporting information can be found online in the Supporting Information section at the end of this article.

How to cite this article: Das T, Pandey VK, Verma S, Pandey SK, Verma B. Optimization of the ratio of aniline, ammonium persulfate, *para*-toluenesulfonic acid for the synthesis of conducting polyaniline and its use in energy storage devices. *Int J Energy Res*. 2022;46(14):19914-19928. doi:10.1002/er.8690

1099114x, 2022, 14, Downloaded from https://onlinelibrary.wiley.com/doi/10.1002/er.8690 by Indian Institute Of Technology, Wiley Online Library on [18/04/2023]. See the Terms and Conditions (https://onlinelibrary.wiley.com/terms-and-conditions) on Wiley Online Library for rules of use; OA articles are governed by the applicable Creative Commons License